

<b>REPORT DOCUMENTATION PAGE</b>				Form Approved OMB NO. 0704-0188	
<p>The public reporting burden for this collection of information is estimated to average 1 hour per response, including the time for reviewing instructions, searching existing data sources, gathering and maintaining the data needed, and completing and reviewing the collection of information. Send comments regarding this burden estimate or any other aspect of this collection of information, including suggestions for reducing this burden, to Washington Headquarters Services, Directorate for Information Operations and Reports, 1215 Jefferson Davis Highway, Suite 1204, Arlington VA, 22202-4302. Respondents should be aware that notwithstanding any other provision of law, no person shall be subject to any penalty for failing to comply with a collection of information if it does not display a currently valid OMB control number.</p> <p>PLEASE DO NOT RETURN YOUR FORM TO THE ABOVE ADDRESS.</p>					
1. REPORT DATE (DD-MM-YYYY)		2. REPORT TYPE New Reprint		3. DATES COVERED (From - To) -	
4. TITLE AND SUBTITLE Maximum-likelihood estimation for frequency-modulated continuous-wave laser ranging using photon-counting detectors				5a. CONTRACT NUMBER W911NF-11-1-0540	
				5b. GRANT NUMBER	
				5c. PROGRAM ELEMENT NUMBER 1D10BQ	
6. AUTHORS Baris I. Erkmen, Zeb W. Barber, Jason Dahl				5d. PROJECT NUMBER	
				5e. TASK NUMBER	
				5f. WORK UNIT NUMBER	
7. PERFORMING ORGANIZATION NAMES AND ADDRESSES Montana State University Office of Contracts and Grants PO Box 172460 Bozeman, MT 59717 -2470				8. PERFORMING ORGANIZATION REPORT NUMBER	
9. SPONSORING/MONITORING AGENCY NAME(S) AND ADDRESS(ES) U.S. Army Research Office P.O. Box 12211 Research Triangle Park, NC 27709-2211				10. SPONSOR/MONITOR'S ACRONYM(S) ARO	
				11. SPONSOR/MONITOR'S REPORT NUMBER(S) 61101-PH-DRP.4	
12. DISTRIBUTION AVAILABILITY STATEMENT Approved for public release; distribution is unlimited.					
13. SUPPLEMENTARY NOTES The views, opinions and/or findings contained in this report are those of the author(s) and should not be construed as an official Department of the Army position, policy or decision, unless so designated by other documentation.					
14. ABSTRACT We analyze the minimum achievable mean-square error in frequency-modulated continuous-wave range estimation of a single stationary target when photon-counting detectors are employed. Starting from the probability density function for the photon-arrival times in photodetectors with subunity quantum efficiency, dark counts, and dead time, we derive the Cramér–Rao bound and highlight three important asymptotic regimes. We then derive the maximum-likelihood (ML) estimator for arbitrary frequency					
15. SUBJECT TERMS ladar, photon statistics, photon counting					
16. SECURITY CLASSIFICATION OF:			17. LIMITATION OF ABSTRACT UU	15. NUMBER OF PAGES	19a. NAME OF RESPONSIBLE PERSON Zeb Barber
a. REPORT UU	b. ABSTRACT UU	c. THIS PAGE UU			19b. TELEPHONE NUMBER 406-994-5925

## Report Title

Maximum-likelihood estimation for frequency-modulated continuous-wave laser ranging using photon-counting detectors

### ABSTRACT

We analyze the minimum achievable mean-square error in frequency-modulated continuous-wave range estimation of a single stationary target when photon-counting detectors are employed. Starting from the probability density function for the photon-arrival times in photodetectors with subunity quantum efficiency, dark counts, and dead time, we derive the Cramér–Rao bound and highlight three important asymptotic regimes. We then derive the maximum-likelihood (ML) estimator for arbitrary frequency modulation. Simulation of the ML estimator shows that its performance approaches the standard quantum limit only when the mean received photons are between two thresholds. We provide analytic approximations to these thresholds for linear frequency modulation. We also compare the ML estimator’s performance to conventional Fourier transform (FT) frequency estimation, showing that they are equivalent if the reference arm is much stronger than the target return, but that when the reference field is weak the FT estimator is suboptimal by approximately a factor of  $\sqrt{2}$  in root-mean-square error. Finally, we report on a proof-of-concept experiment in which the ML estimator achieves this theoretically predicted improvement over the FT estimator.

---

**REPORT DOCUMENTATION PAGE (SF298)**  
**(Continuation Sheet)**

---

Continuation for Block 13

ARO Report Number    61101.4-PH-DRP  
Maximum-likelihood estimation for frequency-mo    ...

Block 13: Supplementary Note

© 2013 . Published in Applied Optics, Vol. Ed. 0 52, (10) (2013), ( (10). DoD Components reserve a royalty-free, nonexclusive and irrevocable right to reproduce, publish, or otherwise use the work for Federal purposes, and to authroize others to do so (DODGARS §32.36). The views, opinions and/or findings contained in this report are those of the author(s) and should not be construed as an official Department of the Army position, policy or decision, unless so designated by other documentation.

Approved for public release; distribution is unlimited.

# Maximum-likelihood estimation for frequency-modulated continuous-wave laser ranging using photon-counting detectors

Baris I. Erkmen,<sup>1,\*</sup> Zeb W. Barber,<sup>2</sup> and Jason Dahl<sup>2</sup>

<sup>1</sup>Jet Propulsion Laboratory, California Institute of Technology, 4800 Oak Grove Drive, Pasadena, California 91109, USA

<sup>2</sup>Spectrum Lab, Montana State University, Bozeman, Montana 59717, USA

\*Corresponding author: baris.i.erkmen@jpl.nasa.gov

Received 11 October 2012; revised 22 January 2013; accepted 15 February 2013;  
posted 21 February 2013 (Doc. ID 177901); published 21 March 2013

We analyze the minimum achievable mean-square error in frequency-modulated continuous-wave range estimation of a single stationary target when photon-counting detectors are employed. Starting from the probability density function for the photon-arrival times in photodetectors with subunity quantum efficiency, dark counts, and dead time, we derive the Cramér–Rao bound and highlight three important asymptotic regimes. We then derive the maximum-likelihood (ML) estimator for arbitrary frequency modulation. Simulation of the ML estimator shows that its performance approaches the standard quantum limit only when the mean received photons are between two thresholds. We provide analytic approximations to these thresholds for linear frequency modulation. We also compare the ML estimator's performance to conventional Fourier transform (FT) frequency estimation, showing that they are equivalent if the reference arm is much stronger than the target return, but that when the reference field is weak the FT estimator is suboptimal by approximately a factor of  $\sqrt{2}$  in root-mean-square error. Finally, we report on a proof-of-concept experiment in which the ML estimator achieves this theoretically predicted improvement over the FT estimator. © 2013 Optical Society of America

*OCIS codes:* 010.3640, 270.5290, 030.5260, 000.5490, 040.1345.

## 1. Introduction

In its essence, optical ranging is a problem of estimating the round-trip flight time of a phase- or amplitude-modulated optical beam that reflects off of a target. Frequency-modulated continuous-wave (FMCW) ranging systems obtain this estimate by performing an interferometric measurement between a local frequency-modulated laser beam and a delayed copy returning from the target. The range estimate is formed by mixing the target-return field with the local reference field on a beam splitter and detecting the resultant beat modulation. In conventional FMCW ranging, the source modulation is linear in instantaneous frequency, the reference-

arm field has many more photons than the target-return field, and the time-of-flight estimate is generated by balanced difference detection of the beam splitter output, followed by a frequency-domain peak search. This technique is known to achieve range resolution proportional to  $c/2\Delta f$  in a  $T$ -second chirp window, where  $c$  is the speed of light,  $\Delta f$  is the chirp bandwidth, and the time-bandwidth product satisfies  $T\Delta f \gg 1$  [1,2].

Important advances have been reported in the recent literature for FMCW ranging systems. To revisit several examples, very broad chirp bandwidths have been achieved using active feedback stabilization [3,4]. Alternative frequency-modulation functions, such as sinusoidal modulation [5,6] and pseudorandom modulation [7], have been employed to improve the range resolution. These results, and much of the literature in general, have focused on the

strong-local-oscillator regime, wherein the mean photon number in the reference field greatly exceeds that in the target-return field over the integration window of interest. A strong local oscillator provides optical gain of a weak target return prior to detection, such that the predominant noise in the photocurrent is the quantum (vacuum) noise of the incident field mode [8,9].

With high efficiency, high bandwidth, and low-noise photon-counting detector technologies rapidly maturing, it is feasible to anticipate that FMCW ranging systems could utilize photon-counting detectors. These detectors offer very high sensitivity, and can accommodate the large bandwidths needed for ranging applications, but their limited dynamic range (i.e., saturation) and their susceptibility to dead time (i.e., blocking) typically precludes the use of a very strong local oscillator. In recent years, there has been interest to quantify the performance attainable with high-sensitivity photon-counting detectors paired with a local oscillator of strength comparable to the target-return signal [10]—that is, a weak local oscillator. In this paper we continue to investigate this question, focusing both on deriving an asymptotically tight lower bound to the estimation accuracy, and on identifying the performance of an estimation algorithm that approaches this bound. Because range is related to time delay by a constant (the speed of light), we present all of our results in terms of the latter and omit the trivial scaling of these results to express them as a range. Our treatment is founded on a rigorous statistical characterization of the (random) photoelectron emission times as a function of the incident optical field, including the deleterious effects caused by dark current and dead time. These statistics permit us to derive the Cramér–Rao lower bound (CRB) on the accuracy of FMCW ranging and to derive the maximum-likelihood (ML) estimator, whose performance approaches this bound under some photon-flux conditions. Here, we determine these conditions and validate the theory via simulation and experiment. Because our emphasis is on FMCW receivers employing photon-counting detectors, we limit the focus of this paper to analyzing the performance when a single specularly reflecting target is present within the range of interest. Nonetheless, the formalism developed herein could be extended to include diffuse target reflections [11], multiple targets within the range of interest [12], and atmosphere-induced distortions [13], with the appropriate modifications to statistics governing the output processes of the photon-counting detectors.

Our paper is organized as follows. In Section 2 we define the problem of interest, and then we derive the CRB for arbitrary frequency modulation. First, we consider only the shot noise of the incident (coherent-state) fields and determine the CRBs achieved by different modulation functions. We then extend our formalism to include dark counts and dead time in the detector, and quantify the degradation in

performance. In Section 3, we derive the ML estimator and show via simulation that when the total mean received photon number is between two thresholds, its mean-square error (MSE) approaches the standard quantum limit. We derive analytic approximations to these threshold values for the case of linear frequency modulation. In addition, we compare the ML estimator’s performance to conventional frequency-domain estimation, highlighting regimes in which they perform identically and regimes in which they do not. Finally, in Section 4, we report on an experiment with linear frequency modulation and compare the results to our analysis.

## 2. Problem Formulation and the Cramér–Rao Bound

Figure 1 illustrates the FMCW ranging system in consideration. We assume that an ideal laser field [14] with center frequency  $\omega_c$  is split via a beam splitter into a signal field  $E_{S,1}(t)e^{-i\omega_c t}$  and a reference field  $E_{R,1}(t)e^{-i\omega_c t}$ , where  $E_{k,1}(t) = \sqrt{N_{k,1}/T}e^{i\phi(t)}$  for  $-T/2 < t \leq T/2$ , and periodically repeating otherwise. The subscript  $k = S, R$  denotes their complex baseband temporal modulations, in which the instantaneous frequency modulation satisfies  $\int_{-T/2}^{T/2} dt \dot{\phi}(t) = 0$ , where  $\dot{\phi}(t) \equiv d\phi(t)/dt$ . In addition,  $E_{k,1}(t)$  are normalized to have units  $\sqrt{\text{photons/s}}$ , such that  $N_{k,1}$  denotes the mean photon number over the  $T$ -second window. The signal field is transmitted to interact with the target, yielding a target-return field  $E_{S,2}(t)$ . In this paper we have assumed a single specularly reflecting target, so  $E_{S,2}(t) = r_S E_{S,1}(t - t_0)$ , where  $r_S \leq 1$  is the field reflection coefficient and  $t_0 \in \mathcal{T}$  is the relative time delay between the signal- and reference-arm fields within the *a priori* domain of uncertainty  $\mathcal{T}$ . The reference-arm field remains local to the ranging instrument, and is therefore assumed to go through a simple attenuation by  $r_R \leq 1$ , yielding  $E_{R,2}(t) = r_R E_{R,1}(t)$ . The receiver mixes the target-return field and the reference field with a 50/50 beam splitter, resulting in

$$E_{D,m}(t) = \frac{E_{S,2}(t) + (-1)^{m+1} E_{R,2}(t)}{\sqrt{2}}, \quad (1)$$

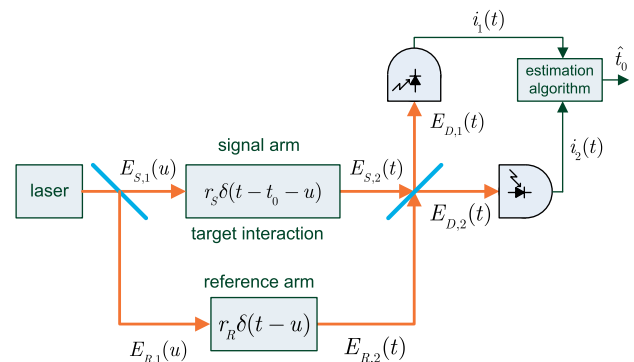


Fig. 1. (Color online) Block diagram of FMCW ranging. Optical fields are denoted with thick (orange) lines and electrical signals are denoted with thin (black) lines.

at its two output ports  $m = 1, 2$ .  $E_{D,m}(t)$  are incident on two matched photon counters for  $t \in (-T/2, T/2]$ , giving rise to the photocurrent processes  $i_m(t)$ . We assume  $i_m(t)$  are normalized by the electron charge to have units photoelectrons/s, and are therefore sequences of unit-area impulses occurring at each photoelectron emission epoch [15]. With ideal laser light incident on the photodetectors,  $i_m(t)$  are independent discrete stochastic point processes whose statistics are governed by several uncertainties. First, energy measurements on coherent-state fields are stochastic due to the quantum nature of light (shot noise) [16]. Second, there are stochastic electron emissions from the photosensitive area of the detector when no light is incident (dark counts). Third, after every photoelectron emission there is a period during which the detector is unable to generate any additional photoelectrons regardless of the incident field amplitude (dead time). The first of these effects is fundamental, whereas the latter two are practical limitations to state-of-the-art photon counters that can be improved upon in the future.

An important component in the Fig. 1 system is the algorithm that generates an estimate  $\hat{t}_0$  of the time delay  $t_0$ , based on the occurrence times of the photoelectrons from the two detectors. Different estimators will achieve different MSE values, an exhaustive characterization of which is not feasible. The CRB, on the other hand, is a lower bound on the MSE achievable by any unbiased estimator [2]. Furthermore, the CRB is achieved by the ML estimator if an efficient estimator exists, and even if one does not exist the ML estimator often asymptotically approaches the CRB at high signal flux. Therefore, we first derive the CRB for the FMCW ranging system described above. Then, we focus on the ML estimator and evaluate its performance relative to the CRB.

#### A. Standard Quantum Limit

Let us first consider near-ideal photon counters and develop some insights into the ultimate performance of FMCW ranging. When  $E_{D,1}(t)$  and  $E_{D,2}(t)$  are incident on matched photon-counting detectors with quantum efficiency  $\eta$ , zero dark current, and zero dead time,  $i_m(t)$  are statistically independent inhomogeneous Poisson point processes with rate functions [9,17,18]

$$\Lambda_m(t; t_0) = \frac{\eta N_I}{2T} [1 + (-1)^{m+1} \beta \cos(D(t; t_0) + \psi_0)], \quad (2)$$

for  $m = 1, 2$ . Here,  $D(t; t_0) \equiv \phi(t) - \phi(t - t_0)$  is the beat modulation that carries information on  $t_0$ , and  $\psi_0 = \omega_c t_0$  denotes the phase shift in the carrier. The parameter

$$\beta \equiv \frac{2\sqrt{N_{S,2}N_{R,2}}}{N_{S,2} + N_{R,2}} \quad (3)$$

is between 0 and 1, indicating the relative strength of the target-return and reference fields in terms of

their mean photon numbers  $N_{k,2} \equiv r_k^2 N_{k,1}$  for  $k = S, R$ , and  $N_I \equiv N_{S,2} + N_{R,2}$  is the total mean number of photons incident on the two detectors. The probability density function for observing  $n_1$  photodetection events in the first detector at event times  $\{u_1, \dots, u_{n_1}\} \in (-T/2, T/2]$  and  $n_2$  photodetection events in the second detector at event times  $\{v_1, \dots, v_{n_2}\} \in (-T/2, T/2]$ , is given by [17]

$$p(n_1, u_1, \dots, u_{n_1}, n_2, v_1, \dots, v_{n_2}; t_0) = \left[ \prod_{i=1}^{n_1} \Lambda_1(u_i; t_0) \right] \left[ \prod_{j=1}^{n_2} \Lambda_2(v_j; t_0) \right] e^{-\int_{-T/2}^{T/2} dt [\Lambda_1(t; t_0) + \Lambda_2(t; t_0)]}. \quad (4)$$

From Eq. (4), the CRB for  $t_0$  is expressed as [2]

$$\text{CRB} \equiv - \left\langle \frac{\partial^2 \log p(n_1, u_1, \dots, u_{n_1}, n_2, v_1, \dots, v_{n_2}; t_0)}{\partial t_0^2} \right\rangle^{-1}, \quad (5)$$

where the angled brackets denote the expectation over all of the random variables.

Throughout this paper we assume that the *a priori* uncertainty in the target range is much greater than an optical wavelength, such that the carrier phase shift  $\psi_0$  provides negligible information in determining the true range. Consequently, to obtain relevant lower bounds on attainable MSE, we ignore the  $t_0$  dependence of  $\psi_0$  by treating it as a constant. In particular, the theoretical derivations below assume  $\psi_0 = 0$  for simplicity. However, in applications that have range uncertainty on the order of a few wavelengths,  $\psi_0$ 's  $t_0$  dependence should be taken into account when calculating Eq. (5).

In Appendix A we show that substituting Eqs. (2) and (4) into Eq. (5) leads to

$$\text{CRB} = \frac{1}{\eta N_I} \left[ \frac{1}{T} \int_{-T/2}^{T/2} dt \frac{\beta^2 \sin^2(D(t; t_0))}{1 - \beta^2 \cos^2(D(t; t_0))} \dot{\phi}^2(t - t_0) \right]^{-1}. \quad (6)$$

For a fixed ratio between the target-return and the reference-arm mean photon numbers, i.e., for  $\beta$  constant, the CRB follows a  $1/N_I$  scaling, which is referred to as the *standard quantum limit* because it is the best possible scaling achievable with photon counting of ideal laser fields. In addition, because the first term in the integrand is maximized at  $\beta = 1$  for all  $t$ , we find

$$\text{CRB} \geq \frac{1}{\eta N_I} \left[ \frac{1}{T} \int_{-T/2}^{T/2} dt \dot{\phi}^2(t - t_0) \right]^{-1}, \quad (7)$$

for all  $N_I \geq 0$  and  $t_0 \in \mathcal{T}$ , with equality if and only if  $\beta = 1$ . Several insights are noteworthy here. First, given a total mean received photon number  $N_I$ , it is optimal to have  $\beta = 1$ , i.e.,  $N_{S,2} = N_{R,2}$ . Second,

**Table 1.**  $\mathcal{L}_2$  Norms of Various Frequency Modulations with Identical Frequency Detuning Range  $\Delta f^a$

Type	$\dot{\phi}(t), t \in (-T/2, T/2]$	$\varepsilon_\phi$
Linear	$\Delta f t / T$	$\Delta f^2 / 12$
Polynomial	$(\Delta f / 2) \text{sgn}(t) (2 t /T)^p, p > 0$	$(\Delta f)^2 / (4(2p + 1))$
Sinusoid	$(\Delta f / 2) \sin(2\pi t / T)$	$\Delta f^2 / 8$
(Pseudo) random	$(\Delta f / 2) \sum_{k=-K}^K a_k b_k(t), a_k \in \{-1, 1\}$	$\Delta f^2 / 4$

<sup>a</sup> $\text{sgn}(t)$  denotes the sign of  $t$ ,  $b_k(t) \equiv 1$  for  $2|t - k\Delta|/\Delta < 1$  and 0 otherwise, where  $T/\Delta \equiv 2K + 1$ , and  $a_k$  are independent and equally likely to take on either value.

Eq. (7) is independent of  $t_0$  when the modulation is periodic with  $T$ . Finally, the optimal CRB depends only on the average energy ( $\mathcal{L}_2$  norm) of the baseband (zero-average) frequency-modulation function. Therefore, frequency modulations with equal  $\mathcal{L}_2$  norm attain the same optimized CRB. Table 1 summarizes the  $\mathcal{L}_2$  norms of several frequency modulations, quantifying their relative performance at equal  $N_I$ .

Setting  $\beta \ll 1$  in Eq. (6), we derive the CRB in the strong-reference-arm regime as

$$\text{CRB} \approx \frac{1}{\beta^2 \eta N_I} \left[ \frac{1}{T} \int_{-T/2}^{T/2} dt \sin^2(D(t; t_0)) \dot{\phi}^2(t - t_0) \right]^{-1}, \quad (8)$$

where the term outside the brackets is approximately equal to  $1/(4\eta N_{S,2})$ . We can now compare the CRBs for  $\beta = 1$  and  $\beta \ll 1$  in several relevant scenarios. If  $N_{S,2}$  is fixed and the reference-arm photon number is allowed to vary, the  $\beta = 1$  and  $\beta \ll 1$  cases yield approximately equal CRBs given by  $1/(2\eta N_{S,2} \varepsilon_\phi)$  [20], where  $\varepsilon_\phi \equiv T^{-1} \int_{-T/2}^{T/2} dt \dot{\phi}^2(t)$ . The former uses fewer photons to achieve this sensitivity but requires photon-counting detectors, whereas the latter uses more photons but could utilize linear-mode detectors. Another relevant scenario is one in which the mean number of source-generated photons is fixed, i.e.,  $N_{S,1} + N_{R,1} = N$ , and these photons are allocated into the signal and reference arms. Assuming the common scenario of high loss along the signal path ( $r_S^2 \ll 1$ ) but low loss along the reference path ( $r_R^2 \approx 1$ ), the CRB for the  $\beta = 1$  case is approximately given by  $1/(2\eta r_S^2 N \varepsilon_\phi)$ , whereas the CRB for the  $\beta \ll 1$  case is approximately  $\gamma/(2\eta r_S^2 N \varepsilon_\phi)$ , with

$$\gamma \equiv 1 + N_{R,1}/N_{S,1} \gg 1 + 4r_S^2 \quad (9)$$

being strictly greater than 1. So, allocating photons such that  $\beta \ll 1$  in general loses relative to having  $\beta = 1$  for  $N$  fixed, but the performance loss is negligible if the mean-photon-number allocation satisfies  $1 \gg N_{R,1}/N_{S,1} \gg 4r_S^2$ .

#### B. Dark Noise and Dead Time

The results above define the best possible performance attainable with ideal laser light and near-ideal photon counting, with subunity quantum efficiency being the only nonideal effect. Now we

add dark counts and dead time to quantify the degradation in the CRB relative to the standard quantum limit. Suppose that the photon-counting detectors from Fig. 1 have equal and constant dark count rates  $\lambda_d$ , but no dead time. Then, the dark counts in each detector form a homogeneous Poisson process with statistics equivalent to having on average  $N_d \equiv \lambda_d T / \eta$  additional photons incident in a  $T$ -second interval. Therefore, the two photodetector outputs are independent inhomogeneous Poisson processes as stated in the previous subsection, but now with the modified rate functions [21]

$$\Lambda_{m,d}(t; t_0) = \frac{\eta N_{I,d}}{2T} [1 + (-1)^{m+1} \beta_d \cos(D(t; t_0))] \quad (10)$$

for  $m = 1, 2$ , where  $N_{I,d} \equiv N_I + 2N_d$  and  $\beta_d \equiv \beta/(1 + 2N_d/N_I)$  are the two parameters that are modified due to dark counts. Next, suppose that the detectors also have equal and deterministic nonparalyzing dead time  $\tau$  [17]. In this case the rate function itself becomes a stochastic process that causally depends on prior arrival times. Consequently, the detector output is modeled as a *self-exciting* point process. The probability density function for observing  $n_1$  photodetection events in the first detector at event times  $\{u_1, \dots, u_{n_1}\} \in (-T/2, T/2]$  and  $n_2$  photodetection events in the second detector at event times  $\{v_1, \dots, v_{n_2}\} \in (-T/2, T/2]$  is now given by [17]

$$p(n_1, u_1, \dots, u_{n_1}, n_2, v_1, \dots, v_{n_2}; t_0) = p_d(n_1, u_1, \dots, u_{n_1}; t_0) p_d(n_2, v_1, \dots, v_{n_2}; t_0), \quad (11)$$

where

$$p_d(n_m, u_1, \dots, u_{n_m}) \equiv \left[ \prod_{i=1}^{n_m} \Lambda_{m,d}(u_i; t_0) \right] \times \exp \left\{ - \int_{-T/2}^{u_1} dt \Lambda_{m,d}(t; t_0) - \sum_{i=2}^{n_m+1} \int_{u_{i-1}}^{u_i} dt \Lambda_{m,d}(t; t_0) w_\tau(t - u_{i-1}) \right\} \quad (12)$$

for  $m = 1, 2$ . Here, we have defined  $u_{n_m+1} \equiv T/2$  for compactness of the expression, and  $w_\tau(t) \equiv 1$  if  $t > \tau$  but is 0 otherwise.

Deriving the CRB is straightforward by substituting Eqs. (11) and (12) into Eq. (5), so we postpone the tedious details to Appendix A. Here we highlight several asymptotes to the CRB expression when the rate of change of  $\Lambda_{m,d}(t; t_0)$  is much slower than  $1/\tau$ , specifically, when the frequency modulation and dead time satisfy  $|\dot{\phi}(t) - \dot{\phi}(t - t_0)|\tau \ll 1$  for all  $t \in (-T/2, T/2]$  and  $t_0 \in \mathcal{T}$ :

$$\text{CRB} \approx \begin{cases} \frac{2N_d(1+\alpha)}{\eta N_I^2 \beta^2} K_1^{-1}(t_0) & N_I \ll 2N_d \text{ and } \alpha \ll 1 \\ \frac{1}{\eta N_I} K_2^{-1}(\beta, t_0) & N_I \gg 2N_d \text{ and } \alpha \ll 1 \\ \frac{\tau}{2T} K_3^{-1}(\beta, t_0) & N_I \gg 2N_d \text{ and } \alpha \gg 1 \end{cases} \quad (13)$$

where  $\alpha \equiv \eta N_{I,d} \tau / (2T)$  is the average fraction of photoelectron counts lost during the dead times, and the three terms independent of photon number are

$$K_1(t_0) = \frac{1}{T} \int_{-T/2}^{T/2} dt \sin^2(D(t; t_0)) \dot{\phi}^2(t - t_0), \quad (14)$$

$$K_2(\beta, t_0) = \frac{1}{T} \int_{-T/2}^{T/2} dt \frac{\beta^2 \sin^2(D(t; t_0))}{1 - \beta^2 \cos^2(D(t; t_0))} \dot{\phi}^2(t - t_0), \quad (15)$$

and

$$K_3(\beta, t_0) = \frac{1}{T} \int_{-T/2}^{T/2} dt \times \frac{\beta^2 \sin^2(D(t; t_0)) [1 + \beta^2 \cos^2(D(t; t_0))]}{[1 - \beta^2 \cos^2(D(t; t_0))]^2} \times \dot{\phi}^2(t - t_0). \quad (16)$$

The asymptotic expressions in Eq. (13) represent three distinct trends with respect to the mean incident photon number. When the mean dark count is significantly greater than the mean signal photon count ( $N_d \gg N_I$ ) and the dead time is short enough to have negligible impact on the arrival rate ( $\alpha \ll 1$ ), the performance is *dark-noise dominated*. In this regime the CRB is significantly worse than the standard quantum limit, and it improves quadratically as the mean incident photon number increases. At the other extreme, when the mean incident photon number is so large that the detector is almost universally blocked by dead time ( $\alpha \gg 1$ ), the output of the photon-counting detectors saturates irrespective of the mean received photon number. Here the performance is *dead-time dominated* and the CRB reaches a floor. Often there is an intermediate regime between these two extremes wherein the signal counts dominate over dark counts ( $N_I \gg N_d$ ), yet the dead time impact is negligible ( $\alpha \ll 1$ ). In this regime the performance is *shot-noise dominated* and the CRB approaches the standard quantum limit. If dark counts or dead time are too high, the ranging performance may never become shot-noise dominated, thus the standard quantum limit may not be attainable.

In Fig. 2 we have plotted the CRB, normalized by  $T^2$  to render it dimensionless, when  $\dot{\phi}(t) = \Delta f t / T$ , i.e., when linear frequency modulation is employed. The dashed curves correspond to the aforementioned asymptotes, and the solid line is the numerically evaluated CRB from Eq. (A6) in Appendix A. The figure indicates that the asymptotes provide a good approximation to the CRB in their applicable regime. Furthermore, the transition thresholds are well-approximated by the intersection points of these asymptotes.

### 3. Maximum-Likelihood Estimation of Range

In this section we derive the ML estimator and show via simulation that its performance approaches the

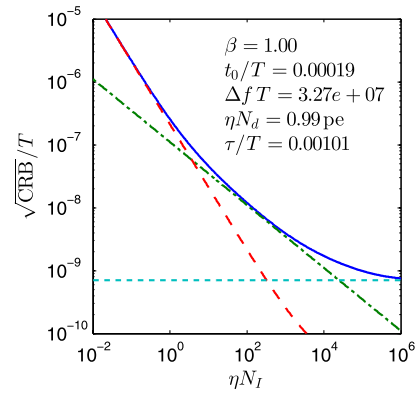


Fig. 2. (Color online) Exact  $\sqrt{\text{CRB}}$ , normalized by  $T$ , is shown as the solid (blue) line. The dashed (red) line is the dark noise asymptote, the dash-dotted (green) line indicates the shot-noise asymptote, and the dotted (cyan) line is the dead-time asymptote.

CRB when the incident photon number satisfies  $N_\ell < N_I < N_u$ , where  $N_\ell$  and  $N_u$  are lower and upper breakdown thresholds, respectively. The lower threshold is due to  $t_0$  having a nonlinear relation to the observation statistics, whereas the upper threshold is due to dead time dominating the observation statistics. We will derive analytic approximations for  $N_\ell$  and  $N_u$  in the case of linear frequency modulation.

The ML estimator is defined as

$$\hat{t}_0 \equiv \underset{t_0 \in \mathcal{T}}{\operatorname{argmax}} \log p(n_1, u_1, \dots, u_{n_1}, n_2, v_1, \dots, v_{n_2}; t_0), \quad (17)$$

where  $\mathcal{T}$  is the support of  $t_0$ . Using the probability density function in Eq. (11) and following straightforward simplifications (see Appendix A for details omitted here), we arrive at

$$\hat{t}_0 = \underset{t_0 \in \mathcal{T}}{\operatorname{argmax}} \int_{-T/2}^{T/2} dt [i_1(t) h_1(t; t_0) + i_2(t) h_2(t; t_0)], \quad (18)$$

where the impulse responses are given by

$$h_m(t; t_0) = \log(1 + (-1)^{m+1} \beta_d \cos(D(t; t_0))) + (-1)^{m+1} \alpha \beta_d \cos(D(t; t_0)), \quad (19)$$

for  $m = 1, 2$ . Thus, a sufficient statistic for the ML estimator is the sum of filtered photodetector outputs, where the filter impulse responses are linear and time varying.

Let us consider several limiting cases of this general estimator. When dead time is negligible, i.e.  $\alpha \ll 1$ , only the first term in Eq. (19) survives, and the impulse responses are recognizable as the log-matched filters to the photoelectron generation rates in each detector. If  $\beta_d \ll 1$  and  $\alpha$  is arbitrary, which occurs with a strong local field ( $\beta \ll 1$ ) or when dark

noise dominates the signal energy ( $N_d \gg N_I$ ), the ML estimator can be simplified as

$$\hat{t}_0 \approx \arg \max_{t_0 \in \mathcal{T}} \int_{-T/2}^{T/2} dt (i_1(t) - i_2(t)) \cos(D(t; t_0)); \quad (20)$$

i.e., difference detection followed by a matched filter to the rate function generates a sufficient statistic. If we further specialize our result to  $\dot{\phi}(t) = \Delta f t / T$ , we obtain

$$\begin{aligned} \hat{t}_0 \approx \arg \max_{t_0 \in \mathcal{T}} & \\ & \times \Re \left\{ e^{i\Delta f t_0^2 / (2T)} \int_{-T/2}^{T/2} du (i_1(u) - i_2(u)) e^{-i\Delta f t_0 u / T} \right\}; \end{aligned} \quad (21)$$

i.e., difference detection followed by a Fourier transform (FT) and peak detection (henceforth referred to as the FT estimator) is also approximately the ML estimator in this regime. This result is not surprising. Both with a strong reference field or with dark-count-dominated noise, the photodetector output processes have a signal-dependent mean but a largely signal-independent noise process. This, together with the (asymptotically tight) approximation that the photodetector outputs form a Gaussian random process when the photoelectron counts are large, yields an additive Gaussian noise channel for which the FT estimator is exactly ML achieving [2].

The equivalence of the two estimators, however, does *not* extend to the  $\beta \approx 1$  regime. To show this, we approximate the term inside the brackets in Eq. (21) as  $S(\Omega - \Omega_0) + N(\Omega)$ , where  $\Omega = \Delta f t_0 / T$  is the normalized variable over which the maximization is performed,  $\Omega_0$  is the true value of the parameter with the same normalization,  $S(\Omega) \equiv \eta N_I \beta \sin(\Omega T / 2) / (\Omega T)$  is the mean, and  $N(\Omega)$  is a zero-mean complex Gaussian random process with the nonzero correlation function  $\langle N^*(\Omega_1) N(\Omega_2) \rangle = (N_I \pi / T) \delta(\Omega_1 - \Omega_2)$ . Using the CRB for estimating  $\Omega_0$  as the true performance of the FT estimator, we arrive at [2]

$$\langle (t_0 - t_0^{(\text{FT})})^2 \rangle \approx 2\text{CRB} \quad (22)$$

for  $\beta = 1$ , where  $t_0^{(\text{FT})}$  denotes the FT estimator, and CRB refers to Eq. (6). Therefore, as the ML estimator's performance approaches the standard quantum limit, we expect that the FT estimator will attain approximately a factor of  $\sqrt{2}$  larger root-mean-square error (RMSE). On the other hand, when  $\beta \ll 1$ , we obtain  $\langle (t_0 - t_0^{(\text{FT})})^2 \rangle \approx \text{CRB}$ , where CRB is now given by Eq. (8), in agreement with our earlier conclusion that the FT and ML estimators are equivalent in this regime.

Figures 3 and 4 plot the simulated MSEs of the ML estimator and the FT estimator for linear frequency modulation as a function of  $\eta N_I$ . Figure 3 represents the near-ideal case with  $N_d = 0$  and  $\tau = 0$  and  $\beta \approx 1$ . We observe that the ML estimator tracks the CRB

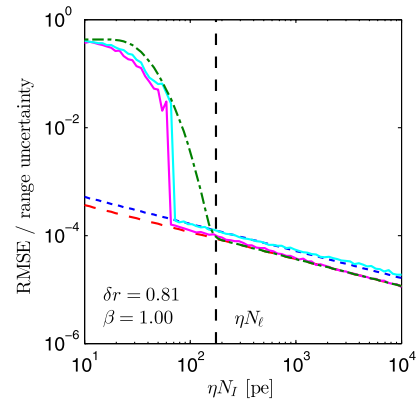


Fig. 3. (Color online) RMSE normalized to the width of the range uncertainty window. The simulated ML (magenta) and FT (cyan) estimator performances, the CRB (dashed red), the analytic RMSE model (dash-dotted green), and the FT RMSE asymptote (dotted blue) are plotted.  $\delta r$  is the fractional position of the object in its support.

well for large values of  $N_I$ . However, when  $N_I$  falls below a threshold, which we denote with  $N_\ell$ , its performance rapidly deteriorates toward a uniformly distributed random guess of  $t_0 \in \mathcal{T}$ . The FT estimator's performance is similar. However, consistent with the derivation in the previous paragraph, its RMSE is approximately a factor of  $\sqrt{2}$  worse than

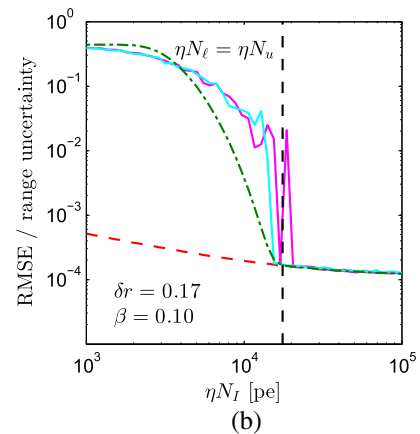
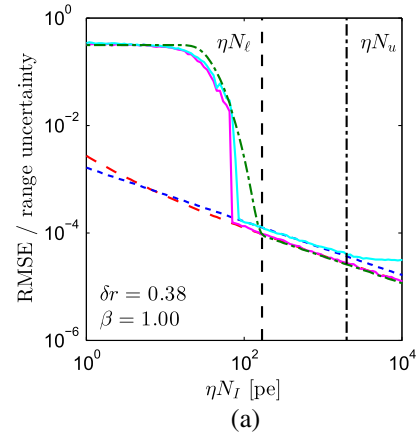


Fig. 4. (Color online) RMSE normalized to the width of the range uncertainty window. Plot legend is identical to that of Fig. 3.

the ML estimator's performance when  $N_I > N_\ell$ . Figure 4(a) includes dark counts and dead time, specifically  $N_d = 1$ ,  $\tau = 100$  ns, and  $\beta \approx 1$ . The qualitative behavior is the same as before: for  $N_I < N_\ell$ , the ML estimator rapidly deteriorates to random uniform guesses, and above this threshold its MSE tracks the CRB. However, unlike the previous case, the CRB itself saturates when  $N_I$  exceeds a threshold we denote as  $N_u$ , causing the MSE to deviate from the standard-quantum-limited scaling of  $1/(\eta N_I)$ . Between these thresholds, where the ML estimator performs at the standard quantum limit, the FT estimator exhibits the  $\sqrt{2}$  gap in RMSE, as expected. Finally, Fig. 4(b) shows a case when  $\beta \ll 1$ . Here, the FT estimator indeed performs very similar to the ML estimator, and its MSE approaches the CRB together with that of the ML estimator. In addition, this case exemplifies a scenario in which only one threshold effect is observed and the ML estimator never achieves the standard quantum limit, because at  $N_I = N_\ell$  the CRB has already deviated from its standard-quantum-limited asymptote. It is evident from these examples that determining  $N_\ell$  and  $N_u$  is critical to identifying the regime in which the ML estimator performs best.

#### A. Lower Threshold $N_\ell$

We will restrict our derivation to the case of linear frequency modulation. Our approach—motivated by prior literature—will be to first introduce an analytic model that approximates the MSE of the ML estimator, and then to derive  $N_\ell$  from this model [22–24]. State-of-the-art photon-counting detectors yield typically better than kilohertz-rate dark counts, which implies no more than low tens of dark counts per realistic integration windows ( $\sim 1$ – $10$  msec). Because we observe that the threshold often occurs at much greater photon numbers, we assume  $N_d \approx 0$  in subsequent derivation. We also assume that  $N_\ell$  occurs in a regime where the photon flux is low enough to warrant the  $\alpha \approx 0$  approximation. We begin by assuming that all possible outcomes can be grouped into two classes of events: (1) *typical* events, i.e., those outcomes that are sufficiently informative and yield average performance close to the CRB, and (2) *atypical* events, i.e., those outcomes that give little to no information and yield average performance close to a random uniform guess of  $t_0 \in \mathcal{T}$ . Based on this classification we write the MSE model for the ML estimator as

$$\langle (t_0 - \hat{t}_0)^2 \rangle = \sigma_A^2 P_A + \text{CRB}(1 - P_A), \quad (23)$$

where the CRB is given by Eq. (A6), but with  $N_d = 0$  and  $\alpha = 0$  it simplifies to the Eq. (6) expression.  $P_A$  denotes the probability that the observed photon-arrival sequence belongs to the atypical set, and

$$\sigma_A^2 \equiv \frac{(T_2 - T_1)^2}{12} + \left( \frac{T_2 + T_1}{2} - t_0 \right)^2 \quad (24)$$

is the MSE of a uniform random guess. Here we have used  $T_1 \equiv \min_{t_0 \in \mathcal{T}} t_0$  and  $T_2 \equiv \max_{t_0 \in \mathcal{T}} t_0$  to denote the end points of  $\mathcal{T}$ . From the Eq. (23) model we define  $N_\ell$  as the  $N_I$  value that satisfies

$$P_A \sigma_A^2 = (1 - P_A) \text{CRB}. \quad (25)$$

Thus, good agreement between the model and the simulated performance hinges on an accurate characterization of  $P_A$ . When the total photoelectron count is zero or one, the ML estimate is uniform over  $\mathcal{T}$ , corresponding to atypical events. So, we can write

$$P_A = P(n < 2) + P(n \geq 2) P_{A|2}, \quad (26)$$

where  $n \equiv n_1 + n_2$  is the total number of counts from both detectors within the observation window,  $P(n < 2) = (1 + \eta N_I) e^{-\eta N_I}$ , and  $P_{A|2}$  denotes the atypical event probability conditioned on two or more arrivals. Unfortunately, it is impractical to ascertain the precise subset of outcomes that are atypical. Therefore, we resort to deriving a tractable approximation to  $P_{A|2}$  in the  $\beta \ll 1$  and  $N_I \gg 1$  limit, and then using it universally.

To evaluate  $P_{A|2}$ , recall from Eq. (21) that for  $\beta \ll 1$  and  $\dot{\phi}(t) = \Delta f t / T$  the cost function has an effective resolution width equal to  $4\pi / \Delta f$ . Dividing  $\mathcal{T}$  into  $n_{\text{bin}} + 1$  bins with centers at  $t_k = T_1 + k4\pi / \Delta f$ , for  $k = 0, \dots, n_{\text{bin}}$ , we approximate  $P_{A|2}$  by

$$P_{A|2} = 1 - P\left(\bigcap_{\ell \neq k^*} C(t_{k^*}) > C(t_\ell)\right), \quad (27)$$

where  $C(t)$  is the cost function given in the argument of the right-hand side of Eq. (21), and  $k^*$  denotes the bin index that contains the true value  $t_0$ . In other words, a typical event occurs if the cost function is peaked at the bin encompassing the true  $t_0$ . A tractable expression for the right-hand side of this equation follows from assuming  $C(t_k)$  are jointly Gaussian random variables. The mean of  $C(t_k)$  is  $\langle C(t_k) \rangle = (\eta N_I \beta^2 / 2) \delta_{k,k^*}$ , and the covariance is given by  $\text{cov}(C(t_k), C(t_\ell)) = (\eta N_I \beta^2 / 2) \delta_{k,\ell}$ , where  $\delta$  is the Kronecker delta function. Consequently, via Eq. (27) we obtain

$$P_{A|2} \approx 1 - \left[ 1 - Q\left(\sqrt{\eta N_I} \beta / 2\right) \right]^{n_{\text{bin}}}, \quad (28)$$

where  $Q(x) \equiv \int_x^\infty dt e^{-t^2/2} / \sqrt{2\pi}$ . Substituting Eq. (28) back into Eq. (26) yields  $P_A$ .

Having evaluated all of the components in Eq. (25), we can solve for  $N_\ell$ . We perform several simplifying approximations to derive a tractable analytic expression. First, via Eq. (6) we use  $\text{CRB}^{-1} \approx \eta N_I \beta^2 \epsilon_\phi$ . Next, we use  $P_A \approx P_{A|2}$  in Eq. (26), and  $(1 - x)^n \approx 1 - nx$  and  $Q(x) \approx e^{-x^2/2} / 2$  in Eq. (28), to solve for the breakdown threshold as

$$N_\ell = -\frac{8}{\eta\beta^2} W_{-1}\left(\frac{-1}{4\varepsilon_\phi\sigma_A^2 n_{\text{bin}}}\right), \quad (29)$$

where  $W_{-1}(y)$  is the Lambert-W function along the  $-1$  branch, formally defined as the inverse of the function  $y = xe^x$  for  $x < -1$  [25].

In Figs. 3 and 4 we have plotted the  $N_\ell$  predicted by Eq. (29), as well as the MSE model from Eq. (23) and the simulation-based MSE. In all three cases, the approximation to  $N_\ell$  matches very well with the knee in the MSE model, indicating that it is a good analytic approximation to the transition in the model. In comparing the model to the simulated MSE results, we find that  $N_\ell$  is higher than the breakdown threshold observed in simulation, but within a factor of three. Therefore, Eq. (29) offers a tractable approximation to the breakdown threshold that conservatively predicts the  $N_I > N_\ell$  region in which the ML estimator may approach the standard quantum limit.

#### B. Upper Threshold $N_u$

Dead time impairs the estimation performance when the average arrival rate of the incident photons significantly exceeds  $1/\tau$ , such that the detectors cannot respond to many information-carrying incident photons. As a result, the CRB—hence the MSE of the ML estimator—starts to saturate when  $N_I > N_u$ . To find the threshold at which this occurs, we return to the CRB asymptotes stated in Eq. (13) and evaluate the  $N_I$  at which the latter two asymptotes intersect. The precise photon-flux threshold at which the CRB begins to deviate from the standard quantum limit is heuristic in nature; however, motivated by the Fig. 2 plot we define it to be a decade prior this intersection value, i.e.,

$$\eta N_u \equiv \frac{K_3(\beta, t_0)T}{5K_2(\beta, t_0)\tau}, \quad (30)$$

where  $K_2$  and  $K_3$  are given in Eqs. (15) and (16), respectively. This expression can be evaluated numerically for a given  $\beta$  and  $t_0$ , but to obtain a simple approximation we use  $K_3 \approx K_2$ , such that

$$N_u \approx \max\left\{\frac{T}{5\eta\tau}, N_\ell\right\}. \quad (31)$$

Here the maximum is due to the fact that if the first term inside the brackets is less than  $N_\ell$ , then atypical events dominate the performance and the dead-time-induced blocking behavior is not visible until  $N_I > N_\ell$ .

The  $N_u$  we have defined above is plotted in the two simulations presented earlier in Fig. 4. In both cases it predicts the regime in which dead time deteriorates the MSE of the ML estimator reasonably well. In Fig. 4(a) the three performance regimes are distinctly identifiable, and the MSE approaches the standard quantum limit only when  $N_\ell < N_I < N_u$ ,

as expected. In Fig. 4(b), on the other hand, we illustrate an  $N_\ell = N_u$  case: when the incident photon flux is sufficiently high to emerge from the regime in which atypical events dominate, it has already become too high for the dead time of the photodetectors. Consequently, the MSE transitions from the first breakdown regime directly into the dead-time-blocked regime, and never achieves the standard quantum limit.

In summary, the ML estimator can achieve the standard quantum limit with the optimal  $1/N_I$  scaling of the MSE, provided that the total mean photon number incident on the two detectors satisfies  $N_\ell < N_I < N_u$ , where  $N_\ell$  is given in Eq. (29) and  $N_u$  is given in Eq. (31). If we have  $N_u = N_\ell$ , then the standard quantum limit is not attainable.

#### 4. Experimental Results

We have performed a proof-of-concept FMCW ranging experiment using linear frequency modulation and photon-counting Geiger-mode avalanche photodiodes (APDs). Here we report on the performance of the ML estimator and discuss insights gained from this experiment.

Figure 5 provides a block diagram of the experimental setup. A linear sawtooth frequency modulation with rate 10.42 GHz/ms and period 3.6 ms is applied to a 1539 nm center-wavelength distributed feedback laser, using active phase locking. 10% of the output power is used in this feedback loop. Furthermore, only the central linearized portion of each period is used in collecting the experimental data, to avoid transients that occur around the sharp frequency transitions. The remaining output power (90%) passes through several attenuators, including a variable attenuator for power adjustment, and 99/1 splitters for power monitoring. An in-line polarizer is used to maintain polarization. This source field is then split into the signal and reference arms via a 50/50 splitter. The signal field passes through a circulator and then is sent out to the target mirror, which is placed approximately 0.8 m away on the optical bench. The return field is recoupled into the circulator and is recombined with the reference field on a 50/50 splitter. The resulting beat frequency is approximately 12.7 kHz, indicating a relative path length of approximately 18 cm. The outputs of the beam splitter are incident on two matched Geiger-mode photon-counting APDs, which have

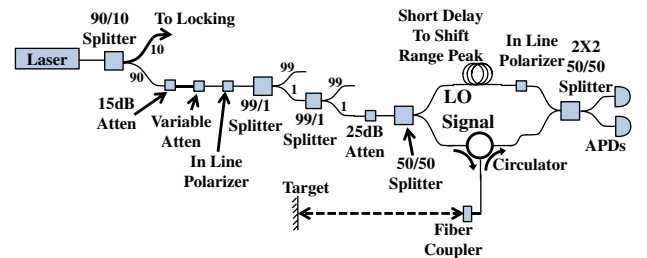


Fig. 5. (Color online) Block diagram of FMCW ranging experiment.

quantum efficiency of  $\eta = 0.1$ , dark noise level  $\lambda_d \approx 1000$  counts/s, and dead time  $\tau \approx 1$   $\mu$ s. The output photoelectrons in each detector are time tagged via a time-to-digital converter unit over a period of  $T = 3.4$  ms. The reference-arm path includes a short delay line for fine adjustments to the beat frequency, and an in-line polarizer to maintain polarization.

The experiment was run at 17 flux levels spanning approximately from 80 to 24,000 mean incident photons per period [26], and at each flux rate approximately 8000 independent data sets were collected. Two estimators were applied to each set, the ML estimator from Eq. (17) and the FT estimator from Eq. (21), but with minor modification to account for the unknown carrier-induced phase shift  $\psi_0$ : in the ML estimator  $\psi_0$  and  $t_0$  were estimated jointly, whereas in the FT estimator the real part of the FT was replaced with its magnitude to render the estimate independent of  $\psi_0$ .

At each photon-flux level the square error in the estimates was averaged to calculate an MSE. A fair assessment of the estimator performance requires an accurate knowledge of the true range to the target. A calibration run with high photon flux (yielding approximately 1600 registered counts per integration window corresponding to approximately 24,000 incident photons) was performed, and the average of the ML estimate and the FT estimate at that photon flux was assumed as the true range to the target [27]. Figure 6 shows the experimental RMSE obtained with the ML estimator and the FT estimator, as a function of  $\eta N_I$ . The CRB and the analytic error model for the ML estimator are also plotted for comparison. Both estimators demonstrate good agreement with the first threshold  $\eta N_\ell$  predicted by the theoretical model. In addition, as predicted by our analysis and simulations in Section 3, the ML estimator's MSE converges to the CRB for  $N_I > N_\ell$ , whereas the FT estimator's MSE is approximately twice the CRB (the observed ratios of the FT estimator's MSE to that of the ML estimator for

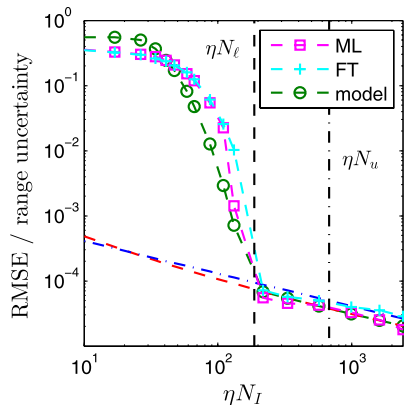


Fig. 6. (Color online) Performance of the ML estimator and the FT estimator, plotted as a function of  $\eta N_I$ . The ML error model, the CRB (dashed red), and the asymptotic RMSE of the FT estimator (dash-dotted blue) are plotted for comparison.

$N_I > N_\ell$  ranges from 1.39 to 2.56). The divergence of the CRB from the standard quantum limit above  $\eta N_u$  is not too pronounced for the range of photon fluxes plotted in the figure, but we observe that the ML estimator's MSE continues to demonstrate good agreement with the CRB above this threshold as the performance transitions to the dead-time-dominated regime. There are two data points close to the  $N_\ell$  threshold in which the ML estimator appears to achieve slightly better performance than the CRB, which we conjecture is a cumulative effect of small errors in estimates of the chirp rate, the observation period, the mean incident photon flux, and the residual statistical error in estimating an ensemble average from a finite sample set.

## 5. Discussion

In this paper we have provided detailed analysis of optimal range estimation using frequency-modulated ideal laser light and continuous-time photon-counting detectors that output time-tagged photon arrivals. Our analysis has centered around three themes: understanding the best possible performance via a study of the CRB, characterizing the performance of the ML estimator, and experimentally validating the theory with a proof-of-concept experiment. The theory that we have developed is sufficiently broad to provide a unified treatment of some of the important recent advances in employing different frequency modulations, as well as varying signal and reference field strengths. It can also be applied to other optical remote-sensing instruments where frequency estimates are calculated from coherently detected fields, e.g., coherent Doppler LIDAR. Our CRB results reveal that the best-case MSE scales as  $1/N_I$ . When the reference-arm mean-photon number is comparable to that of the target return, the primary feature of the (base-band) frequency modulation that impacts the CRB is its average energy, which has permitted us to quantify the gains from employing different modulations. When photodetector dark counts and dead time are included, the CRB admits to three distinct regimes: (1) if dark counts dominate over signal counts, the CRB scales as  $N_d/N_I^2$ ; (2) if the signal counts are high enough to dominate over dark counts but are not so high that dead time blocks the detectors, the standard quantum limit prevails; and (3) if dead time blocks observation of most incident photon arrivals, the CRB is constant with  $N_I$ . Simulating the ML estimator has revealed two thresholds,  $N_\ell$  and  $N_u$ , such that when  $N_\ell < N_I < N_u$ , the performance is approximately equal to the standard quantum limit, but otherwise the performance is bounded away from this optimal scaling. We have derived analytic approximations to these thresholds when linear frequency modulation is used, which identifies the optimal performance regime in terms of critical system parameters. Finally, we have performed an experimental proof of concept with equal reference and target-return field strengths, demonstrating

that the ML estimator behaves as predicted by our analysis, and that it mildly outperforms the RMSE of the FT estimator (approximately a factor of  $\sqrt{2}$ ) at the standard quantum limit.

While the ML estimator has desirable optimality properties, it also has some shortcomings that should be addressed. First, it often has higher implementation complexity, as the cost function to be maximized may not be efficiently computable. In our simulations the ML estimator required seconds to generate an estimate, while the FT estimator's evaluation was subsecond (we did not attempt to optimize either algorithm, but the FT estimator benefited from the computationally efficient fast FT). Second, the ML estimator is more sensitive to auxiliary parameters than the FT estimator, such as  $\beta$  and  $\psi_0$ . Simplifications to the ML estimator are often sought to speed up computation time, reduce complexity, or improve robustness at the expense of some loss in performance. Although here we have not addressed these trades, the FT estimator does emerge as a very good candidate for linear frequency modulation.

In a field-deployed ranging system, several additional uncertainties resulting from the environment are significant. In particular, in this paper we have not considered the effects of rough-surface scattering off of the target, atmospheric turbulence-induced amplitude and phase fluctuations in the target-return signal, ambient background radiation, photo-detector timing jitter, and calibration errors. The theory presented in this paper could be, in principle, extended to encompass these effects by deriving the proper joint probability density function of the photon-arrival times. However, this may prove too complex for tractable and insightful analytic results.

In summary, we have provided a rigorous and detailed analysis of FMCW ranging with ideal laser fields and photon-counting detectors. We have derived the CRB, including the impact of dark counts and dead time. We have shown that the ML estimator can attain the optimal CRB scaling of  $1/N_I$  if the mean received photon number satisfies  $N_e < N_I < N_u$ . We have verified the performance of the ML estimator via a proof-of-concept experiment and shown that it performs better than the conventional FT estimator as predicted by analysis.

## Appendix A: Derivation of Cramér–Rao Bound and ML Estimator

We derive the CRB and the ML estimator for general dark count rate and dead time. Setting these parameters to zero yields the near-ideal results in Section 2. Consider a pair of matched photon-counting detectors in the Fig. 1 setup, having quantum efficiency  $\eta$ , mean dark rate  $\lambda_d$  (in photoelectrons/seconds) and dead time  $\tau$  (in seconds). In the following derivation we will use  $\Lambda_{m,d}(t) \equiv \Lambda_{m,d}(t; t_0)$  to keep our notation compact.

Taking the logarithm in Eq. (11) yields

$$\begin{aligned} \log p(n_1, u_1, \dots, u_{n_1}, n_2, v_1, \dots, v_{n_2}; t_0) \\ = \log f_1 + \log f_2 + C_1, \end{aligned} \quad (\text{A1})$$

where we have omitted a constant term independent of  $t_0$ . In the limit that the rate functions  $\Lambda_{m,d}(t)$  vary slowly over the duration  $\tau$ , i.e., when  $|dD(t; t_0)/dt|\tau \ll 1$ , we have

$$\log f_m \approx \int_{-T/2}^{T/2} dt i_m(t) (\log \Lambda_{m,d}(t) + \tau \Lambda_{m,d}(t)). \quad (\text{A2})$$

Substituting Eq. (A2) into Eq. (A1), and that into Eq. (5), yields

$$\begin{aligned} \text{CRB}^{-1} = \sum_{m=1}^2 \int_{-T/2}^{T/2} dt \langle i_m(t) \rangle \\ \times \left[ \frac{\dot{\Lambda}_{m,d}^2(t)}{\Lambda_{m,d}^2(t)} - \frac{\ddot{\Lambda}_{m,d}(t)}{\Lambda_{m,d}(t)} - \tau \ddot{\Lambda}_{m,d}(t) \right], \end{aligned} \quad (\text{A3})$$

where we have used the shorthand notation  $\Lambda_{m,d}(t) \equiv d\Lambda_{m,d}(t)/dt_0$  and  $\ddot{\Lambda}_{m,d}(t) \equiv d^2\Lambda_{m,d}(t)/dt_0^2$ .

The last step of evaluating the CRB is to find  $\langle i_m(t) \rangle$ . In general, this expectation is difficult to derive for self-exciting stochastic processes. However, when the rate function varies slowly relative to the dead-time interval, it has been shown that the average photocurrent is expressible as [28]

$$\langle i_m(t) \rangle = \frac{\Lambda_{m,d}(t)}{1 + \tau \Lambda_{m,d}(t)}. \quad (\text{A4})$$

This mean arrival rate has intuitive asymptotes. When  $\tau \Lambda_{m,d}(t) \ll 1$ , we have  $\langle i_m(t) \rangle \approx \Lambda_{m,d}(t)$ , indicating that the impact of dead time is negligible. On the other hand, if  $\tau \Lambda_{m,d}(t) \gg 1$ , the detector is continually blocked by arrivals occurring every  $\tau$  seconds, so the mean arrival rate converges to  $\langle i_m(t) \rangle \approx 1/\tau$ .

Substituting Eq. (A4) into (A3), recognizing that  $\dot{\Lambda}_1(t) = -\dot{\Lambda}_2(t)$  and  $\ddot{\Lambda}_1(t) = -\ddot{\Lambda}_2(t)$ , and some straightforward algebraic manipulation results in

$$\begin{aligned} \text{CRB}^{-1} = \int_{-T/2}^{T/2} dt \dot{\Lambda}_{1,d}^2(t) \left[ \sum_{m=1}^2 \frac{1}{\Lambda_{m,d}(t)(1 + \tau \Lambda_{m,d}(t))} \right]. \end{aligned} \quad (\text{A5})$$

Finally, substituting the Eq. (10) rate functions into this expression, we arrive at

$$\text{CRB} = \frac{T}{\eta N_{I,d}} \left[ \int_{-T/2}^{T/2} dt \frac{\beta_d^2 \sin^2(D(t; t_0))}{1 - \beta_d^2 \cos^2(D(t; t_0))} \dot{\phi}^2(t - t_0) \right. \\ \left. \times \frac{1 + \alpha[1 + \beta_d^2 \cos^2(D(t; t_0))]}{1 + 2\alpha + \alpha^2[1 - \beta_d^2 \cos^2(D(t; t_0))]} \right]^{-1}, \quad (\text{A6})$$

where  $\alpha = \eta N_{I,d} \tau / (2T)$ . The Eq. (13) asymptotes follow from considering the corresponding limits of this expression. To obtain the standard quantum limit stated in Eq. (6), we set  $N_d = 0$  and  $\alpha = 0$ .

To derive the ML estimator, we start with the logarithm of the probability density function that we have derived above. Substituting Eqs. (A1) and (A2) into Eq. (17), followed by some straightforward simplifications of the expressions, yields the linear filtering form of Eq. (18) with the impulse responses specified in Eq. (19).

The authors thank the anonymous reviewers for their detailed feedback, which has greatly improved the manuscript. BIE's contributions to the research described in this paper were supported by the DARPA InPho, contract PROP. 81-17433, and were carried out by the Jet Propulsion Laboratory, California Institute of Technology, under a contract with the National Aeronautics and Space Administration. ZWB's and JD's contributions were supported by DARPA InPho, Army Research Office Grant W911NF-11-1-0540.

## References and Notes

1. M.-C. Amann, T. Bosch, M. Lescure, R. Myllylä, and M. Rioux, "Laser ranging: a critical review of usual techniques for distance measurement," *Opt. Eng.* **40**, 10–19 (2001).
2. H. L. V. Trees, *Detection, Estimation and Modulation Theory, Part 1* (Prentice Hall, 2001).
3. N. Satyan, A. Vasilyev, G. Rakuljic, V. Leyva, and A. Yariv, "Precise control of broadband frequency chirps using optoelectronic feedback," *Opt. Express* **17**, 15991–15999 (2009).
4. Z. W. Barber, W. R. Babbitt, B. Kaylor, R. R. Reibel, and P. A. Roos, "Accuracy of active chirp linearization for broadband frequency modulated continuous-wave lidar," *Appl. Opt.* **49**, 213–219 (2010).
5. L. T. Masters, M. B. Mark, and B. D. Duncan, "Analysis of lidar range resolution enhancement by sinusoidal phase modulation," *Opt. Eng.* **34**, 3115–3121 (1995).
6. D. Dupuy, M. Lescure, and M. Cousineau, "A FMCW laser range-finder based on a delay line technique," in *Proceedings of IEEE Instrumentation and Measurement Technology Conference* (IEEE, 2001), pp. 1084–1088.
7. K. Asaka, Y. Hirano, K. Tatsumi, K. Kasahara, and T. Tajime, "A pseudo-random frequency modulation continuous wave coherent lidar using an optical field correlation detection method," *Opt. Rev.* **5**, 310–314 (1998).
8. H. P. Yuen and V. W. S. Chan, "Noise in homodyne and heterodyne detection," *Opt. Lett.* **8**, 177–179 (1983).
9. L. Mandel and E. Wolf, *Optical Coherence and Quantum Optics* (Cambridge University, 1995).
10. L. A. Jiang and J. X. Luu, "Heterodyne detection with a weak local oscillator," *Appl. Opt.* **47**, 1486–1503 (2008).
11. T. J. Green and J. H. Shapiro, "Maximum-likelihood laser radar range profiling with the expectation-maximization algorithm," *Opt. Eng.* **31**, 2343–2354 (1992).
12. S. Hernandez-Marin, A. M. Wallace, and G. J. Gibson, "Bayesian analysis of lidar signals with multiple returns," *IEEE Trans. Pattern Anal. Mach. Intell.* **29**, 2170–2180 (2007).
13. T. J. Karr, "Atmospheric phase error in coherent laser radar," *IEEE Trans. Antennas Propag.* **55**, 1122–1133 (2007).
14. Throughout this paper, an *ideal laser field* refers to a paraxial and quasi-monochromatic optical field in a single spatial and polarization mode, which is also in a coherent state of the quantized field operator, such that it gives rise to Poisson statistics when an ideal photon-counting measurement is performed on it [9].
15. This characterization of the photodetector output implies that the detector has infinite electrical bandwidth, allowing the arrival times to be precisely resolvable. In practice, there is little loss in adopting this idealization if the photodetector impulse response is significantly narrower than the mean photoelectron interarrival time.
16. R. M. Gagliardi and S. Karp, *Optical Communications* (Wiley, 1976).
17. D. L. Snyder, *Random Point Processes* (Wiley, 1975).
18. Tensor-product coherent states incident on a beam splitter yield tensor-product coherent-state outputs [19]. Because the propagation paths in Fig. 1 can be modeled as a sequence of beam splitters (including the loss elements), the fields incident on the photodetectors will also be tensor-product coherent states. It is well known that in this case the semi-classical theory of photodetection and quantum measurement theory predict exactly the same statistics for the output photocurrent [9].
19. Z. Y. Ou, C. K. Hong, and L. Mandel, "Relation between input and output states for a beam splitter," *Opt. Commun.* **63**, 118–122 (1987).
20. The square-bracketed term in Eq. (8) is approximated as  $\epsilon_\phi/2$  to obtain this result.
21. Here we continue to assume  $\psi_0 = 0$ , consistent with our treatment in the previous section.
22. P. Forster, P. Larzabal, and E. Boyer, "Threshold performance analysis of maximum likelihood DOA estimation," *IEEE Trans. Signal Process.* **52**, 3183–3191 (2004).
23. F. Athley, "Threshold region performance of maximum likelihood direction of arrival estimators," *IEEE Trans. Signal Process.* **53**, 1359–1373 (2005).
24. B. I. Erkmen and B. Moision, "Maximum likelihood time-of-arrival estimation of optical pulses via photon-counting photodetectors," in *Proceedings of IEEE International Symposium on Information Theory* (IEEE, 2009), pp. 1909–1913.
25. R. M. Corless, G. H. Gonnet, D. E. G. Hare, D. J. Jeffrey, and D. E. Knuth, "On the Lambert W function," *Adv. Comput. Math.* **5**, 329–359 (1996).
26. The mean incident photon number,  $N_I$ , is estimated from the mean registered photoelectron counts,  $n_{\text{det}}$ , by accounting for the incident photons lost to dead time.  $n_{\text{det}}$  is equal to the sum and integral of the mean arrival rates given in Eq. (A4) in Appendix A. To a good degree of approximation,  $n_{\text{det}} = \eta N_I (1 + \alpha(1 - \beta^2/2)) / (1 + 2\alpha + \alpha^2(1 - \beta^2/2))$ .
27. The (appropriately normalized) mean of the two estimators at this flux level are separated by approximately 1 Hz, whereas the standard deviation of the estimates is on the order of 10 Hz. Thus, the contribution of the bias term to the MSE is negligible as long as the true range to the target is in the vicinity of the mean estimates generated by the two estimators. We believe that both estimators having significant bias at the highest flux level is unlikely.
28. G. Vannucci and M. C. Teich, "Effects of rate variation on the counting statistics of dead-time-modified Poisson processes," *Opt. Commun.* **25**, 267–272 (1978).